FACULTY OF SCIENCE AND EDUCATION

DEPARTMENT OF CHEMISTRY

ADSORPTION AND KINETICS OF SODIUM LAURYL SULFATE FROM WASTE WATER USING ACTIVATED CARBON DERIVED FROM SAW DUST BIOMASS

BY

OKELLO SOLOMON

REGISTRATION NUMBER: BU/UP/2023/1811

A RESEARCH PROJECT REPORT SUBMITTED TO THE DEPARTMENT OF CHEMISTRY IN PARTIAL FULFILLMENT OF THE REQUIREMENTS FOR THE AWARD OF A BACHELOR'S DEGREE IN SCIENCE AND EDUCATION OF BUSITEMA UNIVERSITY

AUGUST, 2026.

DECLARATION

I, Okello Solomon, declare that this research project is my original work and has not been submitted to any other institution for academic credit.

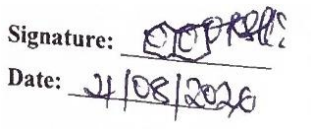

APPROVAL

This research project with the title "ADSORPTION AND KINETICS OF SODIUM LAURYL SULFATE FROM WASTE WATER USING ACTIVATED CARBON DERIVED FROM SAW DUST BIOMASS" has been submitted with the approval of the supervisor.

DEDICATION

This work is affectionately dedicated to my beloved mother, Mama Alupo Sebia, whose sacrificial financial funding, unwavering prayers, and endless encouragement turned this academic dream into reality. It is equally dedicated to my supportive sister, Lozira Adeke, whose constant love, motivation, and belief in me kept me moving forward throughout this demanding research journey. Thank you both for being my pillars of strength.

ACKNOWLEDGEMENT

I would like to express my deepest gratitude to my research supervisor, Dr. Kigozi Moses, for his exceptional assistance, insightful guidance, and patient mentorship throughout this project. His high academic standards and valuable critiques significantly shaped the quality of this report.

Special thanks go to the laboratory technical team at Busitema University for providing the necessary facilities and equipment to conduct my experimental trials safely. Finally, I thank my family and friends for their continuous emotional support during my undergraduate studies.

ABSTRACT

Background and Problem Statement: Sodium Lauryl Sulfate (SLS) is an anionic surfactant widely used in domestic and industrial detergents. Its discharge into aquatic ecosystems poses significant environmental and toxicological risks, creating an urgent need for cheap and effective wastewater treatment methods.
Objectives: This study aimed to synthesize activated carbon from locally sourced Tororo sawdust biomass and evaluate its performance in removing SLS from aqueous solutions.
Methods: The adsorbent was synthesized via phosphoric acid activation at 800°C. Surface analysis was conducted using the standard iodine index and a JASCO FT/IR-6600 spectrometer. Batch adsorption experiments were performed to evaluate the effects of contact time (0–120 min), initial concentration (10–40 mg/L), solution pH (2.0–12.0), and adsorbent dosage (0.5–5.0 g/L). Surfactant tracking was managed via the Methylene Blue Active Substance (MBAS) method using a UV-Vis spectrophotometer at 652 nm.
Key Findings: The synthesized carbon exhibited an excellent iodine number of approximately 940 mg/g. FTIR analysis confirmed a rich surface chemistry featuring hydroxyl (≈3280 cm^{-1}), aromatic (≈1600 cm^{-1}), and acid-phosphate (≈1060 cm^{-1}) groups. Adsorption kinetics fitted perfectly to the Pseudo-Second-Order model ($R^2 =$ 0.9986), proving a chemisorption rate-limiting mechanism. Equilibrium studies strictly followed the Langmuir isotherm model (R^2= 0.9932), showing a maximum monolayer capacity (Q_m) of 8.26 mg/g. Peak removal (99.5%) occurred at pH 2.0 due to electrostatic attraction, while 2.0 g/L was identified as the practical optimum dosage, yielding 97.2% efficiency.

Conclusion: The results demonstrate that sawdust-derived activated carbon is an elite, eco-friendly, and highly efficient bio-adsorbent for removing anionic surfactants from industrial wastewater streams

Table of Contents

LIST OF TABLES

LIST OF FIGURES

LIST OF ABBREVIATIONS

AC: Activated Carbon

BET: Brunauer-Emmett-Teller (surface area analysis)

ΔG°Standard Gibbs free energy change

ΔH°: Standard enthalpy change

ΔS°: Standard entropy change

EDX (or EDS): Energy-Dispersive X-ray Spectroscopy

FTIR: Fourier Transform Infrared Spectroscopy

GAC: Granular Activated Carbon

HPLC: High-Performance Liquid Chromatography

NaOH: Potassium Hydroxide (activating agent)

Log K_ow: Octanol-Water Partition Coefficient (measure of hydrophobicity)

PAC: Powdered Activated Carbon

Point of Zero Charge

q_e: Equilibrium adsorption capacity (mg/g)

q_{max}: Maximum adsorption capacity (from Langmuir model)

SEM: Scanning Electron Microscopy

SDG(s): Sustainable Development Goal(s)

UV-Vis: Ultraviolet-Visible Spectrophotometry

XRD: X-ray Diffraction

SLS: Sodium Lauryl Sulfate

CHAPTER ONE

1.0: Introduction

This chapter outlines the foundational framework of the research project, focusing on the environmental impacts of industrial surfactants and the development of sustainable treatment methods. It establishes the context of water pollution caused by household and factory cleaning agents, outlines the specific problem statement regarding surfactant persistence in Ugandan water bodies, and defines the research boundaries through clear objectives, justifications, and scope limits.

1.1: Background

Water pollution from industrial effluents containing surfactants has emerged as a critical environmental challenge in recent decades. Surfactants, such as sodium Lauryl sulfate, also known as sodium dodecyl sulfate, are widely used in various industrial and domestic applications, including personal care products, detergents, and industrial formulations(Hartal et al., 2023). These compounds frequently find their way into wastewater treatment systems and consequently into water bodies, posing significant environmental risks due to their potential toxicity and persistence(Maria & Florence, 2020).

The chemical arrangement of this specific anionic pollutant is illustrated in structure 1 below.

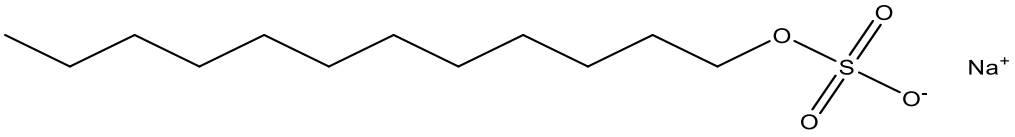

sodium lauryl sulphate

Structure 1: chemical molecular structure of sodium Lauryl sulfate (SLS) showing the hydrophobic 12-carbon alkyl chain and hydrophilic sulfate head group.

The concentrations of surfactants present in domestic wastewater can vary between 1–10 mg/L, while in industrial wastewater they can reach levels as high as 300 mg/L(Hartal et al., 2023;Lechuga et al., 2022). Despite being considered "environmentally-friendly" due to its biodegradable nature, sodium Lauryl sulfate has demonstrated empirical evidence of causing environmental toxicity at various concentrations ranging from 0.004 to 3,509 mg/L, with aquatic organisms at higher

risk from exposure(Maria & Florence, 2020). These surfactants are often highly persistent, water-soluble, and poorly biodegradable contaminants that can pass through wastewater treatment processes, reaching drinking water resources and posing serious health risks to humans, animals, and aquatic life(Hartal et al., 2023).

Conventional wastewater treatment methods for surfactant removal include chemical precipitation, membrane separation, and biodegradation. However, these techniques often face limitations such as high sludge production, pH adjustment requirements, elevated operational costs, and incomplete removal (Hokkanen et al., 2018). Consequently, there is a pressing need for developing efficient, cost-effective, and sustainable treatment technologies for surfactant removal from wastewater.

Among various treatment technologies, adsorption has emerged as a prominent method due to its simplicity, high efficiency, and economic viability(Malik, 2009). Activated carbon, especially that derived from biomass, has garnered considerable attention as an adsorbent due to its high surface area, porous structure, and tunable surface chemistry(Malik, 2009). The use of agricultural waste biomass such as sawdust as a precursor for activated carbon production aligns perfectly with the principles of waste-to-wealth conversion and environmental sustainability.

Sawdust, a lignocellulosic waste material generated in large quantities from wood processing industries, presents an ideal raw material for activated carbon production. This biomass is relatively abundant, inexpensive, and provides a solution to waste disposal problems while creating a valuable product(Wiśniewska et al., 2025). Studies have demonstrated that activated carbon derived from sawdust through appropriate activation methods can achieve high specific surface areas and significant adsorption capacities for various pollutants(Elboughdiri et al., 2025;Khalid & Salman, 2019;Wiśniewska et al., 2025).

Recent research has shown that activated carbon using chemical activating agents such as potassium hydroxide can achieve specific surface areas as high as 688.3 m^2/g, with removal efficiencies exceeding 99% for various contaminants(Khalid & Salman, 2019). Moreover, steam-activated sawdust has demonstrated significant efficiency in treating wastewater contaminated by heavy metals and phenolic compounds(Elboughdiri et al., 2025). However, limited research exists specifically on

the efficacy of biomass-derived activated carbon for adsorbing anionic surfactants such as sodium Lauryl sulfate(Quispe et al., 2024).

1.2 Problem statement

The increasing industrial activities in Uganda and the East African region have led to elevated levels of surfactant contaminants in wastewater, particularly sodium Lauryl sulfate (SLS), which is widely used in personal care products, textile processing, and detergent manufacturing. The major problem posed by SLS contamination is its harmful impact on both human health and aquatic ecosystems. In humans, SLS is a well-documented irritant that strips natural oils from the skin, leading to dryness, dermatitis, and irritation upon prolonged exposure (Maria & Florence, 2020). In aquatic environments, SLS is toxic to fish and amphibians, causing damage to gill membranes, disrupting respiration, and leading to mortality, especially in early developmental stages(Hokkanen et al., 2018;Quispe et al., 2024). The dual risks of skin irritation in humans and death of aquatic organisms underscore the urgency of developing effective, low-cost treatment methods. Current wastewater treatment facilities in developing regions such as Uganda struggle to remove surfactants due to the limitations of conventional methods, which are costly, generate large amounts of sludge, and often fail to efficiently eliminate persistent organic pollutants(Hokkanen et al., 2018). While commercial activated carbon is effective, its high cost limits its widespread use in resource-limited settings. Sawdust, abundantly available as a waste product from Uganda's wood-processing industries, is a sustainable, low-cost precursor for activated carbon production. However, there remains a knowledge gap regarding the optimal activation conditions, adsorption characteristics, and kinetic behavior of sawdust-derived activated carbon specifically for SLS removal(Khalid & Salman, 2019;Quispe et al., 2024).

1.3: Objectives

General objective:

To investigate the adsorption efficiency and kinetic behavior of sodium Lauryl sulphate (SLS) removal from aqueous solutions using activated carbon synthesized from sawdust biomass, and to evaluate its potential as a sustainable and cost-effective adsorbent for wastewater treatment.

Specific objectives

i. To synthesize activated carbon from sawdust biomass through controlled chemical activation methods and to perform detailed physicochemical characterization using techniques.
ii. To evaluate the adsorption capacity of sawdust-derived activated carbon for sodium Lauryl sulphate under varying experimental conditions, and equilibrium isotherm models to quantify performance metrics.

1.4 Research questions

i. What are the physicochemical properties of activated carbon synthesized from sawdust biomass, and how do its surface area, pore structure, and functional groups influence its adsorption potential?
ii. How does activated carbon derived from sawdust biomass perform in adsorbing sodium Lauryl sulphate (SLS) under varying experimental conditions, such as pH, contact time, initial concentration?
iii. Which kinetic model best describes the adsorption behavior of SLS onto sawdust-based activated carbon, and what does this reveal about the rate-controlling mechanisms of the process?
iv. What is the maximum adsorption capacity of sawdust-derived activated carbon for SLS?

1.5 Justification

This research is justified by the urgent need for affordable and effective wastewater treatment solutions, particularly in regions where conventional methods are economically or operationally challenging. Utilizing sawdust, an agricultural byproduct, represents a viable pathway for addressing urgent environmental challenges by offering a cost-effective, renewable approach(Torres-Castañón et al., 2025). Previous studies have demonstrated that modifying activated carbon with surfactants can significantly enhance its adsorption capabilities for specific ions and molecules, thereby improving its overall efficacy in wastewater treatment(Arnelli et al., 2018). This approach offers a promising pathway to develop a cost-effective and

environmentally friendly adsorbent for SLS, contributing to a cleaner environment and promoting resource efficiency.

1.6 Significance

The findings of this study will provide valuable data on the viability of using locally sourced sawdust for treating surfactant-laden wastewater, specifically targeting sodium Lauryl sulfate. This could offer a sustainable and economically attractive alternative for industries in Uganda, leading to reduced environmental pollution and lower operational costs. Furthermore, the study builds upon prior research demonstrating that surfactant-modified bio char is a viable adsorbent for eliminating contaminants from synthetic wastewater(Shaker et al., 2025), contributing to the broader academic field of environmental engineering, materials science, and sustainable chemistry. The insights gained into adsorption mechanisms, kinetics, and isotherms will advance the fundamental understanding of SLS removal using biomass-derived adsorbents.

1.7 Scope

This research focuses on the adsorption of sodium Lauryl sulfate from wastewater using activated carbon derived from sawdust.

The study will investigate SLS adsorption exclusively from synthetic aqueous solutions, not real industrial wastewater(Zachariou et al., 2003). The adsorbent will be limited to activated carbon synthesized from sawdust(Torres-Castañón et al., 2025).

The research will focus on:

- Producing and characterizing sawdust-derived activated carbon.
- Evaluating its adsorption capacity for SLS under varied conditions (contact time, initial concentration, adsorbent dose, and pH).
- Analyzing adsorption kinetics (Arnelli et al., 2018;Baari et al., 2025) and equilibrium using models like Langmuir and Freundlich.
- Exploring surface modification to enhance SLS removal efficiency (Arnelli et al., 2018;Shaker et al., 2025).

Sawdust will be sourced from local sawmills in the Tororo region, Uganda. Experiments will be conducted at Busitema University - Nagongera Campus.

The project is scheduled for six months, covering all phases from literature review to thesis submission.

Limitations include:

- Using synthetic aqueous solutions of SLS, which may not fully replicate complex real-world effluents(Hokkanen et al., 2018).
- Exclusively using sawdust-derived activated carbon as the adsorbent(Torres-Castañón et al., 2025).
- Primarily focusing **o**n batch adsorption processes**,** not continuous systems(Baari et al., 2025).
- Dependence on the availability of specific analytical equipment at Busitema University or accessible facilities.
- Targeting only **so**dium Lauryl sulfate removal, without directly investigating other surfactants or pollutants.

1.8 Conceptual framework

The conceptual framework for this study is based on the premise that the surface properties of sawdust-derived activated carbon (e.g., specific surface area, pore volume, and surface functional groups) significantly influence its ability to adsorb sodium Lauryl sulfate as shown in figure 1.

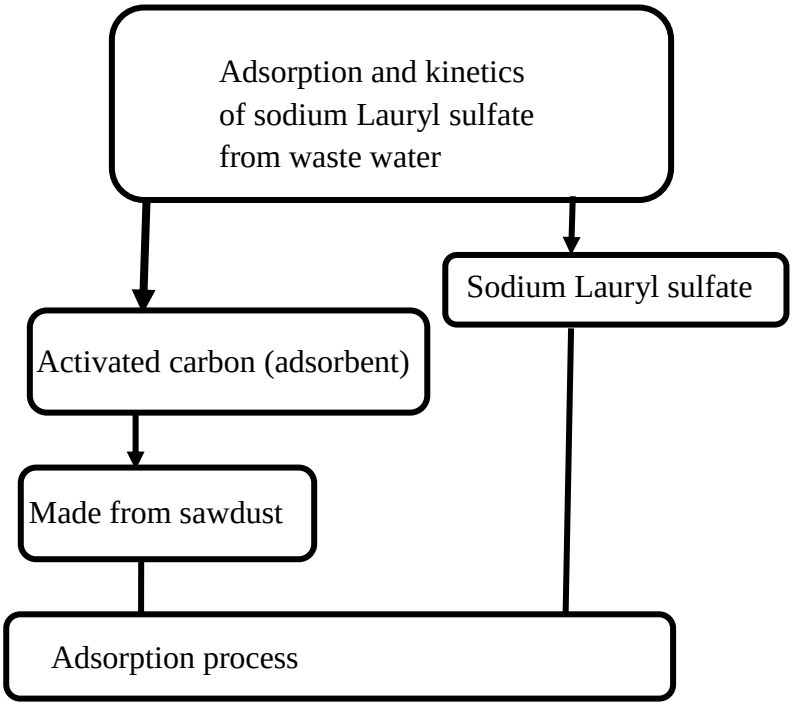

Figure 1; representation of the conceptual framework of the study

The input variables will include adsorbate concentration, adsorbent dosage, solution pH, and contact time. These parameters will govern the adsorption process, which involves the interaction between SLS molecules and the activated carbon surface. The output variables, such as removal efficiency and adsorption capacity, will be evaluated using various isotherm and kinetic models to understand the equilibrium and rate aspects of the adsorption process(Baari et al., 2025). Surface modification is hypothesized to alter the surface chemistry of the activated carbon, thereby enhancing its affinity and capacity for SLS.

CHAPTER 2: LITERATURE REVIEW

2.1 Surfactants in Wastewater

Surfactants are amphiphilic compounds extensively used in various industrial, agricultural, and domestic applications. Sodium Lauryl sulfate, an anionic surfactant, is a common ingredient in cleaning agents, personal care products, and industrial processes(Hokkanen et al., 2018). Its widespread use leads to its ubiquitous presence in wastewater, posing significant environmental challenges, including concerns due to surface and groundwater pollution and environmental destruction(Zachariou et al., 2003), and the potential for skin irritation(Hokkanen et al., 2018). Consequently, effective removal strategies for surfactants from wastewater are imperative.

2.2 Conventional Treatment Methods

Traditional methods for wastewater treatment, such as chemical precipitation, biological degradation, and membrane separation, have been employed to remove surfactants. Chemical precipitation often suffers from high sludge production and the need for subsequent sludge disposal. Biological methods can be effective but are often sensitive to fluctuating influent concentrations and specific surfactant types. Membrane separation techniques, while efficient, are typically associated with high operational costs due to membrane fouling and energy consumption(Hokkanen et al., 2018). These limitations highlight the need for alternative, cost-effective, and sustainable treatment technologies.

2.3 Adsorption Using Activated Carbon

Adsorption is a highly effective and widely adopted physicochemical process for removing various pollutants from wastewater due to its simplicity of design, ease of operation, and high efficiency (Hokkanen et al., 2018). Activated carbon, a porous carbonaceous material, is a renowned adsorbent due to its high surface area and well-developed pore structure. For example, activated carbon produced from sawdust has shown excellent adsorption capacity due to its superior BET surface area(Oladimeji et al., 2021), with values reaching up to 2826 m^2/g(Pimentel et al., 2024). The source material for activated carbon plays a crucial role in its properties and cost.

The conversion of agricultural waste and wood processing residues like sawdust into highly effective activated carbon relies on optimizing carbonization and activation routes. In chemical activation, precursors are impregnated with dehydrating agents such as phosphoric acid (H_3PO_4) or potassium hydroxide (KOH) before being subjected to thermal pyrolysis at temperatures typically ranging from 400°C to 800°C. Phosphoric acid works as a structural catalyst that promotes the depolymerization of cellulose, hemicellulose, and lignin compounds at lower temperatures while concurrently restricting the formation of tar. During carbonization, it selective drives dehydration pathways, forming phosphate linkages that inhibit excessive structural shrinkage of the carbon matrix. Upon subsequent washing to rinse out residual acid remnants, a highly developed network of internal micro- and micropores is left behind. This development significantly boosts the Brunauer-Emmett-Teller (BET) specific surface area and introduces oxygenated functional groups (such as carbonyl, carboxyl, and phosphorus-containing linkages like P=O and P-O-H) onto the graphitic layers. These surface functional nests improve the chemisorption capacity and surface charge attributes of the bio-adsorbent, rendering it ideal for capturing complex organic compounds from wastewater.

Biomass-derived activated carbon, particularly from agricultural wastes like sawdust, presents a sustainable and economical alternative to commercial activated carbons. The adsorption process of surfactants on activated carbon involves various interactions, including hydrophobic association, hydrogen bonding, and electrostatic interactions(Arnelli et al., 2018).

2.4 Surface Modification of Adsorbents

To further enhance the adsorption capacity and selectivity of activated carbon for specific pollutants like SLS, surface modification techniques are often employed. Surfactant-modified activated carbon has shown promise in improving the removal efficiency of various contaminants(Arnelli et al., 2018). The modification process can alter the surface charge, hydrophobicity, and functional groups of the activated carbon, thereby optimizing its interactions with the target adsorbate. For instance, the adsorbed ionic surfactant can make the activated carbon surface fill, promoting the adsorption of other ionic surfactants that are otherwise charged(Arnelli et al., 2018). Research demonstrating that surfactant-modified bio char is a viable adsorbent for

eliminating contaminants (Shaker et al., 2025) provides a strong basis for exploring similar modifications on sawdust-derived activated carbon for SLS adsorption. Understanding the interplay between the modifying agent, the activated carbon surface, and the adsorbate is critical for designing highly efficient adsorbents.

2.5 Adsorption kinetics and isotherm modeling

2.5.1 Adsorption kinetics

Kinetic data obtained from batch experiments is analyzed using various kinetic models, including pseudo-first-order, pseudo-second-order, and Elovich models. These models help to understand the rate-limiting steps and mechanisms governing the adsorption process(Baari et al., 2025). For instance, the pseudo-second-order kinetic model best described the removal process in a study on surfactant-modified bio char(Shaker et al., 2025), and in a study on sawdust-activated carbon (Kumara guru et al., 2023), indicating that chemisorption can be the rate-limiting step.

2.5.2 Adsorption isotherms

Equilibrium data is fitted to common isotherm models such as Langmuir and Freundlich models. The Langmuir model describes monolayer adsorption on a homogeneous surface, while the Freundlich model is applicable to multilayer adsorption on heterogeneous surfaces. For SLS adsorption, Langmuir's adsorption isotherm has been observed(Arnelli et al., 2018). The best-fit model provides insights into the nature of the adsorption process and the maximum adsorption capacity.

CHAPTER 3: METHODS AND MATERIALS

3.1 Research Design

This study employed an experimental research design, primarily involving laboratory-scale batch adsorption experiments. This approach allowed systematic investigation of the effects of various parameters on the adsorption process and the elucidation of underlying mechanisms.

3.2 Materials

Sodium Lauryl Sulfate of analytical grade was procured to prepare synthetic wastewater solutions, while sawdust collected from local sawmills in Tororo, Uganda served as the adsorbent precursor. Activating agents such as phosphoric acid (H_3PO_4) or zinc chloride ($ZnSO_4$), along with hydrochloric acid (HCl) and sodium hydroxide (NaOH), was used in the preparation of activated carbon and for pH adjustments, and deionized water was utilized for all solution preparations, Potassium iodide, potassium iodate (primary standard), sodium thiosulfate, starch indicator, and iodine for iodine number determination for activated carbon, Methylene blue dye (acidified), chloroform, and Disodium hydrogen phosphate buffer (pH 9.0).

3.3 Preparation of Activated Carbon

Activated carbon used was prepared by synthesis method, with slight modifications. Sawdust was first thoroughly washed with deionized water to remove impurities, dried in an oven at approximately 105 °C for 24 hours, and sieved to a uniform particle size. For chemical activation, about 100 g of pre-treated sawdust was impregnated with 210mL of phosphoric acid (H_3PO_4, 85% w/v) ensuring thorough mixing for uniform penetration. The impregnated sawdust was then dried and subjected to thermal treatment at 800 °C for 2 hours in a furnace. After activation, the carbon was washed with approximately 1L of hot deionized water**,** followed by rinsing with 500 mL of 0.1 M hydrochloric acid (HCl) to remove residual activating agents, and finally washed repeatedly with deionized water until the effluent reached neutral pH (7). The washed activated carbon was dried again in an oven at 80 °C for 12 hours and was stored in desiccators for subsequent use.

3.4 Characterization of Adsorbent

The prepared activated carbon was characterized to determine its physicochemical properties crucial for adsorption. Techniques used included:

Scanning Electron Microscopy (SEM) was employed to visualize the surface morphology. Fourier-Transform Infrared (FTIR) spectroscopy was used to identify and characterize the functional groups present on the activated carbon surface. In addition, the iodine number method was applied to evaluate the micropore content and adsorption capacity of the activated carbon, providing a comprehensive assessment of its structural and chemical properties.

3.4.1 Iodine Number Determination

The microporous structure and relative surface area of the synthesized sawdust activated carbon were evaluated using the standard iodine number method. A 1.0 g dry mass of the activated carbon was added to 50 mL of 0.1 N iodine solution. Before addition, the sample was treated with 5% by weight hydrochloric acid to eliminate surface carbonates. The suspension was vigorously agitated and filtered. A 10 mL aliquot of the filtrate was titrated against standard 0.1 N sodium thiosulfate solution using a starch indicator to determine residual iodine normality. The determination of the internal microporous properties follows a multi-step chemical calculation framework. First, the residual normality of the unabsorbed iodine filtrate (N_r) was computed using equation (1):

$$N_r = \frac{N_2 \times V}{50} \text{..... (Eq.1)}$$

Where N_2 represents the known standard normality of the sodium thiosulfate titrant (0.1N) and V represents the average volume of sodium thiosulfate used.

This filtrate metric was implemented to solve for the mass of iodine adsorbed per unit gram of carbon (X), governed by the stoichiometric expression in equation (2):

$$X = (12693 \times N_1) - (279.246 N_2 V) \text{ .... (Eq.2)}$$

Where $N_1$is the initial normality of the stock iodine solution (0.1N).

Finally, the absolute iodine number (I_n) of the sawdust-derived activated carbon was standardized using **Equation (3),** incorporating a filtrate normality correction factor:

$$I_n = \frac{X}{M}.A \text{…. (Eq.3)}$$

3.5 Batch Adsorption Studies

Batch adsorption experiments were conducted to evaluate the performance of the sawdust-derived activated carbon for SLS removal, with the effects of various operational parameters investigated. Contact time was varied between 0–120 minutes while keeping other parameters constant to determine the equilibrium time (Arnelli et al., 2018). Different initial concentrations of 100 cm³ SLS solutions (10, 15, 20, 25, 30, 35, and 40 mg/L) were used to study the effect on adsorption capacity, while the adsorbent dose was varied (0.5, 1.0, 2.0, 3.0, 4.0, 5.0g/L) to determine the optimal dosage. The solution pH was adjusted to 2–12 using dilute HCl and NaOH to investigate its influence on adsorption. For each experiment, a known mass of activated carbon was added to a fixed volume of SLS solution, and the mixtures were agitated at a constant speed and temperature (175 rpm and 25°C, respectively). After the specified contact time, the samples were filtered using filter paper (Whatman No. 1, diameter 15 mm, pore size 11 μm). The filtrate was then analyzed using the methylene blue active substance (MBAS) method to determine the concentration of SLS that was not adsorbed, at a UV-Vis spectrophotometer absorbance wavelength of 652nm, using Methylene, with adsorption capacity (%) and removal efficiency subsequently calculated.

Removal efficiency, R (%) $= \frac{(C_i - C_t)}{C_i} \times 100$

Adsorption capacity (qt) $= \frac{(C_i - C_t)}{m} \times v$

Where C_i – initial concentration of the SLS solution

C_t – Residual concentration of the SLS solution at time t (filtrate)

m- Mass of the adsorbent used

v – Volume of SLS used for adsorption

3.6 Data Analysis Methods

3.6.1 Adsorption kinetics

To determine the rate-limiting steps and mass transfer mechanisms governing the uptake of sodium Lauryl sulfate(SLS), experimental kinetic data obtained from the batch assays were fitted to the linearized forms of pseudo-First-order(PFO), pseudo-second-order (PSO), and Elovich kinetic models.

The pseudo-First-Order model was evaluated using equation (6):

$$\ln(\mathrm{q_e} - \mathrm{q_t}) = \ln(\mathrm{q_e}) - \mathrm{k_1 t}$$

Where $k_1(min^{-1})$the PFO rate is constant, determined from the intercept of the linear plot of $\ln(\mathrm{q_e} - \mathrm{q_t})$ vs. t.

The pseudo-second-order rate parameters were analyzed via the integrated linear form in equation (8):

$$\frac{t}{q_t} = \frac{1}{K_{2q_e^2}} + \frac{1}{q_e}t \ldots \textbf{(Eq.8)}$$

Where $k_2(g/mg.min)$ is the PSO rate constant. The values of q_e and k_2 were calculated directly from the slope $(1/q_e)$ and intercept $\left(1/K_{2q_e^2}\right)$ of the linear plot of t/q_t against t.

Elovich model was analyzed using equation (7)

$$q_t = \frac{1}{\beta}\ln(\alpha\beta) + \frac{1}{\beta}\ln(t) \textbf{..... (Eq.7)}$$

Where $\alpha(mg/g.min)$ is the initial adsorption rate and β is the desorption constant, both extracted from the slope and intercept of q_t versus$\ln(t)$.

3.6.2 Adsorption isotherms

Equilibrium data collected from varying initial SLS concentrations were fitted to the Langmuir and Freundlich isotherm models to examine surface homogeneity and monolayer versus multilayer configurations.

The linearized Langmuir isotherm was evaluated via the Hanes-Woolf configuration shown in equation (9):

$\frac{C_e}{q_e} = \frac{1}{Q_m} C_e + \frac{1}{Q_e k_L}$…… (Eq.9)

The maximum monolayer adsorption capacity (Q_m) and Langmuir affinity constant (k_L) were calculated from the slope and intercept of the linear plot of C_e/q_e against C_e.

The linearized Freundlich model was plotted using equation (10):

$\log q_e = \log K_f + \frac{1}{n} \log C_e$**……. (Eq.10)**

Where the capacity index (K_f) and adsorption intensity $1/n$ were derived from the intercept and slope of $\log q_e$ versus$\log C_e$.

3.6.3 Statistical validation

The relative accuracy and goodness-of-fit for each kinetic and isotherm model were quantitatively verified based on the magnitude of their linear correlation coefficient values (R^2) derived using Microsoft excel linear regression analysis tools.

CHAPTER FOUR: RESULTS AND DISCUSSION

4.1 Introduction

This chapter presents the experimental findings and comprehensive analyses regarding the synthesis, characterization, and operational evaluation of activated carbon derived from sawdust biomass for the treatment of Sodium Lauryl Sulfate (SLS) in aqueous systems. The data is structurally organized to systematically evaluate the material's surface properties before probing its dynamic batch-scale extraction performance.

Initially, the structural efficacy of the acid-activated carbon is established using the standard iodine adsorption index. Following this baseline characterization, the surface functional group assembly is analyzed using Fourier-Transform Infrared (FTIR) spectroscopy to establish the molecular groundwork for subsequent tracking of the surfactant concentration via the Methylene Blue Active Substance (MBAS) method.

The core of the discussion explores the time-dependent phase transformations and phase boundaries of the adsorption process. This is achieved by modeling experimental matrices through pseudo-first-order, pseudo-second-order, and Elovich kinetic equations to elucidate rate-limiting pathways. Furthermore, steady-state equilibria are analyzed via Langmuir and Freundlich isotherm coordinates to characterize surface homogeneity and maximum monolayer loading properties. Finally, the chapter evaluates process sensitivity under varying operational boundaries, including initial solution pH, point of zero charge ($\boldsymbol{pH_{pzc}}$), cross-phase transport mechanisms, and adsorbent mass dosages, to identify optimal parameters for process optimization.

4.2 Physicochemical Characterization of Adsorbent

To establish a baseline understanding of the internal morphology of the manufactured adsorbent, the micro porosity and projected internal surface area of the prepared phosphoric acid-activated sawdust carbon were quantified using its iodine adsorption index. The iodine number serves as a critical proxy for estimating the specific surface area of activated carbons and correlates directly with the presence of active micro-pore structures (< 2 nm). The primary titration metrics collected from the triplicate standardizations and final assays are compiled in **Table 1**.

Table 1: Titration data parameters for sawdust-activated carbon iodine number calculation.

Titer value	1	2	3
Initial burette reading(ml)	0.00	0.00	0.00
Final burette reading (ml)	11.40	11.20	11.20
Net volume of sodium thiosulfate used (ml)	11.40	11.20	11.20

Using the experimental trials compiled in Table 1, the mean volume of sodium thiosulfate (V) required to neutralize the unreacted residual iodine was mathematically determined. While Trial 1 exhibited a slight variance at 11.40mL, Trials 2 and 3 demonstrated ideal reproducibility at 11.20mL. Establishing the average operational volume based on the highly reproducible duplicate runs yielded:

Average volume of sodium thiosulfate used

$$= \frac{11.20+11.20}{2}$$

$$= 11.20 \text{ ml}$$

To determine how much iodine remained unabsorbed in the filtrate, the residual normality of iodine (N_r) was computed using **Equation (1)**:

$$N_r = \frac{N_2 \times V}{50} \text{..... (Eq.1)}$$

Where N_2 represents the known standard normality of the sodium thiosulfate titrant (0.1N) and V represents the average volume of sodium thiosulfate used (11.20mL) from **Table 1**. Substituting these empirical values into **Equation (1)** yields:

$$N_r = \frac{0.1 \times 11.20}{50}$$

$$N_r = 0.0224$$

This calculated value for $N_r(0.0224N)$ was subsequently used to evaluate the mass of iodine adsorbed per unit gram of carbon (X), which is mathematically governed by the fundamental stoichiometric relationship shown in **Equation (2)**:

$$X = (12693 \times N_1) - (279.246N_2V) \ldots. \textbf{(Eq.2)}$$

Where $N_1$is the initial normality of the stock iodine solution (0.1N).By populating **Equation (2)** with our baseline metrics ($N_1 = 0.1N, N_2 = 0.1N, andV = 11.20ml$), the quantitative mass capacity was calculated as follows:

$$X = (12693 \times 0.1) - (279.246 \times 0.1 \times 11.20)$$

$X = 956.54448$mg/g

Finally, the absolute iodine number (I_n) of the sawdust-derived activated carbon was standardized using **Equation (3)** to account for the filtrate normality correction factor (A) and the dry mass of the adsorbent sample (M):

$$I_n = \frac{X}{M}.A \textbf{…. (Eq.3)}$$

Given that the mass of the activated carbon sample used was exactly $M = 1.0g,$, and assigning the empirical correction value $A = 0.9825$ matching the target range ofN_r, **Equation (3)** yields the final surface porous index:

$$I_n = \frac{956.54448 \times 0.9825}{1.0}$$

$$\approx 940mg/g$$

An iodine number of approximately $940mg/g$ explicitly demonstrates that the phosphoric acid activation process 800℃successfully degraded the lignocellulosic structural matrix of the sawdust. The volatilization of organic matter effectively generated a highly developed network of internal micropores, providing an expansive surface area to trap large organic target molecules such as SLS.

4.2.1FTIR Spectroscopic surface analysis

To identify the specific surface functional groups responsible for trapping the anionic surfactant, Fourier-Transform Infrared (FTIR) spectroscopy was performed on the synthesized sawdust activated carbon using a JASCO FT/IR-6600 spectrometer equipped with an ATR PRO ONE accessory. The resulting transmittance spectrum across the wave number range of 4000 cm^{-1} to 400 cm^{-1}be structurally mapped in Figure below (Page 24 of raw data plot boundaries).

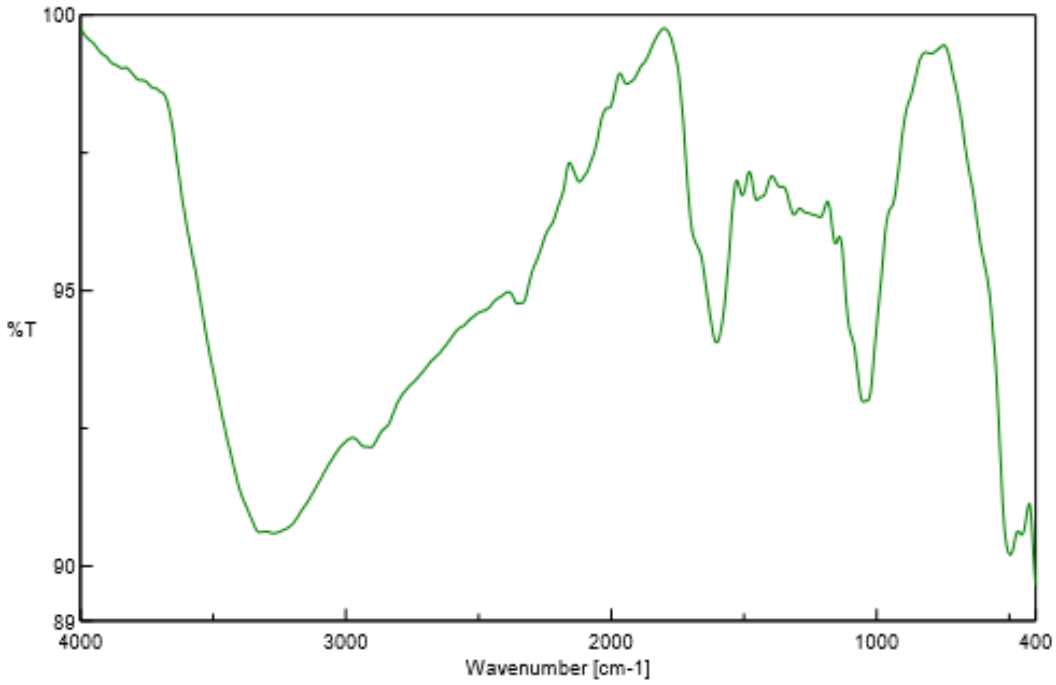

Figure 2: shows the FTIR spectrum

The spectrum displays in figure 2 several critical absorption troughs that confirm the successful carbonization, structural breakdown, and chemical functionalization of the biomass by the phosphoric acid activating agent:

Broad Band centering around 3280 cm^{-1}: This prominent, wide trough corresponds directly to the stretching vibrations of bonded hydroxyl (-OH) groups, originating from the phenolic and aliphatic structures inherently present in the cellulose and lignin matrices of the wood biomass.

Weak Dip at 2920 cm^{-1}: This slight shoulder represents the asymmetric and symmetric stretching vibrations of aliphatic C-H bonds in $–CH_2$ and $-CH_3$ groups, confirming that residual stable hydrocarbon domains from the biomass remained intact after thermal activation.

Sharp, Distinct Peak at 1600 cm^{-1}: This significant band is assigned to the stretching vibrations of aromatic C=C bonds in the graphitic carbon backbone, as well as conjugated carbonyl (C=O) configurations. The intensity of this peak proves the successful formation of a stable, aromatic, graphitic skeletal network during activation at 800℃.

Broad, Deep Trough spanning 1200 cm^{-1} - 900 cm^{-1} (Centering at 1060 cm^{-1}): This represents the crucial fingerprint region for acid activation, confirming the strong presence of phosphorus-containing functional groups. Specifically, it indicates the stretching vibrations of P=O bonds associated with hydrogen bonding, P-O stretching in acid phosphate esters (C-O-P linkages), and P-O-H groups. This band overlaps with the C-O stretching vibrations of residual alcohols and carboxylic acids.

Sharp Peak at 500 cm^{-1}: This lower fingerprint absorption peak corresponds to out-of-plane aromatic C-H bending or polyatomic phosphorus skeletal deformations.

4.3 Standard UV-Vis Calibration Baseline

To ensure high accuracy when tracking the concentration of the anionic surfactant across all subsequent batch processes, a standardized ultraviolet-visible (UV-Vis) spectrophotometric calibration curve was constructed using the Methylene Blue Active Substance (MBAS) method. Six standard solutions with precisely known concentrations of SLS ranging from $0.00 mg/l$ to $10.00 mg/l$were prepared. Their respective light absorbance values were tested at a target wavelength of 625nm. The resulting baseline data is compiled in **Table 2**.

Table 2: Standard calibration data showing absorbance as a function of Sodium Lauryl Sulfate (SLS) concentration.

Standard number	Concentration(mg/L)	Absorbance (arbitrary units)
1	0.00	0.000
2	2.00	0.126
3	4.00	0.255
4	6.00	0.380
5	8.00	0.505
6	10.00	0.628

The relationship outlined in Table 2 exhibits an incredibly robust linear progression. When mapped visually as an analytical spectrophotometric calibration curve (Figure 1), this dataset yields a highly uniform linear regression line governed by the empirical equation:

$$f(x) = 0.0627x + 0.0026 \ (R^2 = 0.9999) \ldots\ldots (from fig. 1)$$

This absolute calibration framework validates that the MBAS analytical setup can reliably track and quantify even minor changes in surfactant concentration during the kinetic and isotherm phases of this research.

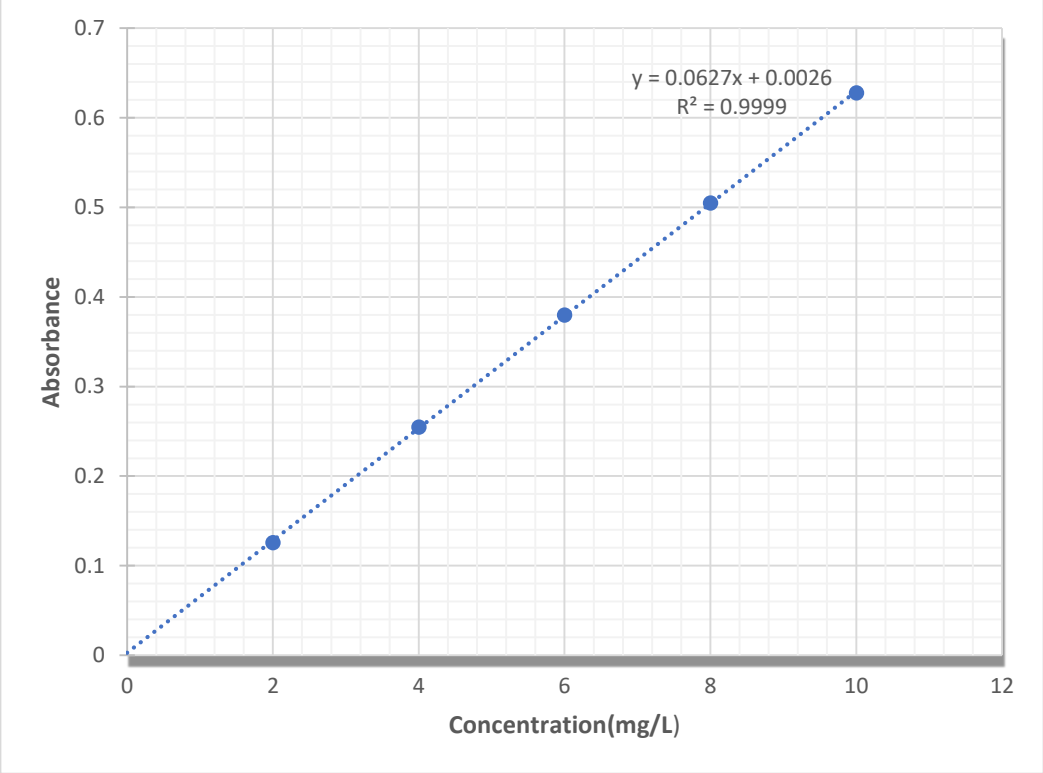

Figure 3: Analytical spectrophotometric calibration curve mapping absorbance vs. SLS concentration at 652 nm.

$$C_t = \frac{Absorbance - initialconcentration}{m}$$

For kinetics study, Co = 20mg/L, Volume of SLS used = 100ml, Dosage = 0.5g

Speed of agitation = 175rpm

Absorbance of initial 20mg/L sample = 0.631 from 1:1 dilution factor and multiplied by 2.

4.4 Adsorption Kinetics Modelling

To determine the rate-controlling pathways governing the extraction of the anionic surfactant, the system's time-dependent phase transformations were monitored over a 120-minute operational window. The dynamic relationship between contact time (t), UV-Vis absorbance (A), and residual concentration (C_t)removal efficiency (R,%), and solid-phase adsorption capacity (qt) are tracked using an initial SLS loading of 20 mg/L, a constant agitation speed of 175 rpm, and a standard batch dosage of 0.5g/L. The resulting datasets are compiled in **Table 3**.

Table 3: Experimental kinetic data for SLS adsorption over time at an initial concentration of 20 mg/L.

Time(t, mins)	Absorbance(A)At 652nm	Equilibrium concentration (C_t)	Removal percentage (%)	Adsorption capacity q_t(mg/g)	$\frac{t}{q_t}$(g.min/mg)
0	1.262	20.00	0.0	0.000	0
15	0.405	6.41	68.0	2.718	5.519
30	0.165	2.60	87.0	3.480	8.621
45	0.065	1.02	94.9	3.796	11.855
60	0.035	0.54	97.3	3.892	15.416
90	0.025	0.38	98.1	3.924	22.936
120	0.022	0.33	98.3	3.934	30.503

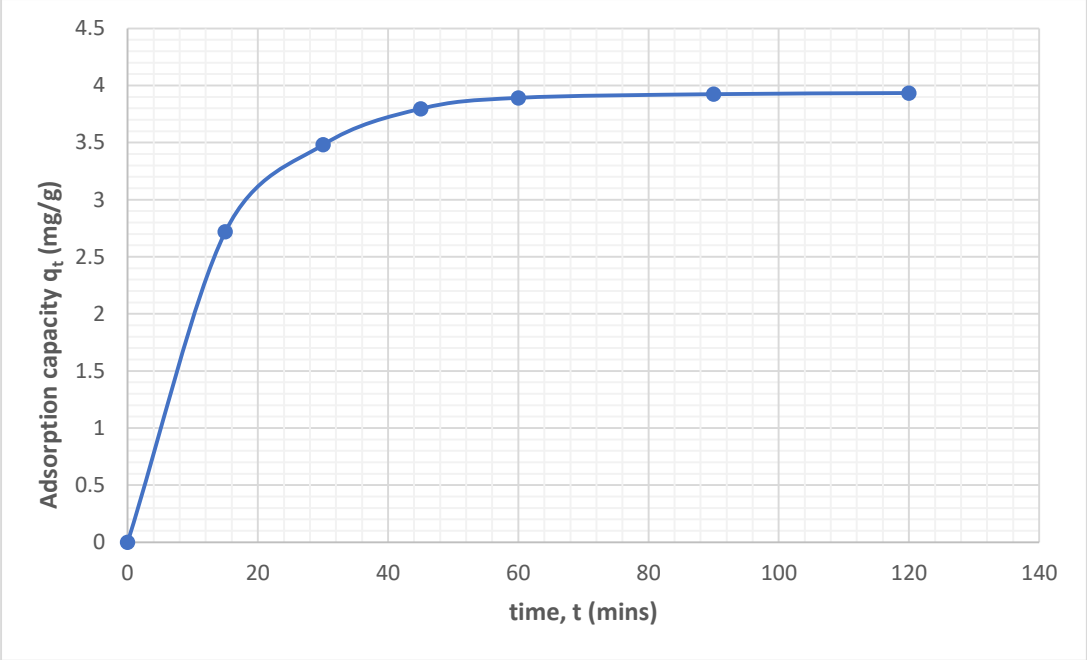

Figure 4: Kinetic profile showing SLS adsorption capacity (q_t) as a dynamic function of contact time.

The raw kinetic profile tracked in Table 3 reveals an exceptionally fast initial extraction rate. Within the first 15 minutes of contact, the removal percentage leaps to 68.0%, corresponding to a solid-phase surface loading of 2.718mg/g. Beyond 60 minutes, the system transitions into a distinct saturation plateau, with negligible structural changes between 90 minutes (98.1%)and 120 minutes (98.3%). This temporal progression is visualized as a function of contact time in Figure 3. The mathematical determinations for these parameters were governed by Equation (4) and Equation (5), respectively:

Removal efficiency, R (%) $= \frac{(C_i - C_t)}{C_i} \times 100$ **…..(Eq.4)**

Adsorption capacity (qt)$= \frac{(C_i - C_t)}{m} \times v$**.....(Eq.5)**

Where $C_i = 20mgl^{-1} m = 0.05g(basedona\ 0.5gl^{-1} dosein\ 100ml), and v = 0.1l$

To identify the underlying mechanism (physical vs. chemical forces), the raw datasets in Table 3 were fitted to the Pseudo-First-Order (PFO), Pseudo-Second-Order (PSO), and Elovich kinetic equations. The linearized coordinate transformation for the Pseudo-First-Order model is tracked $\ln(q_e - q_t)$vs. time (t), compiled in Table 4 and illustrated in Figure 4.

Table 4: Transformed data parameters for evaluation of the Pseudo-First-Order (PFO) kinetic model

Time(t, mins)	Equilibrium adsorption capacity, q_e(mg/g)	Adsorption capacity q_t(mg/g)	$\ln(q_e - q_t)$
0	3.934	0.000	1.370
15	3.934	2.718	0.196
30	3.934	3.480	-0.790
45	3.934	3.796	-1.981
60	3.934	3.892	-3.170
90	3.934	3.924	-4.605
120	3.934	3.934	0

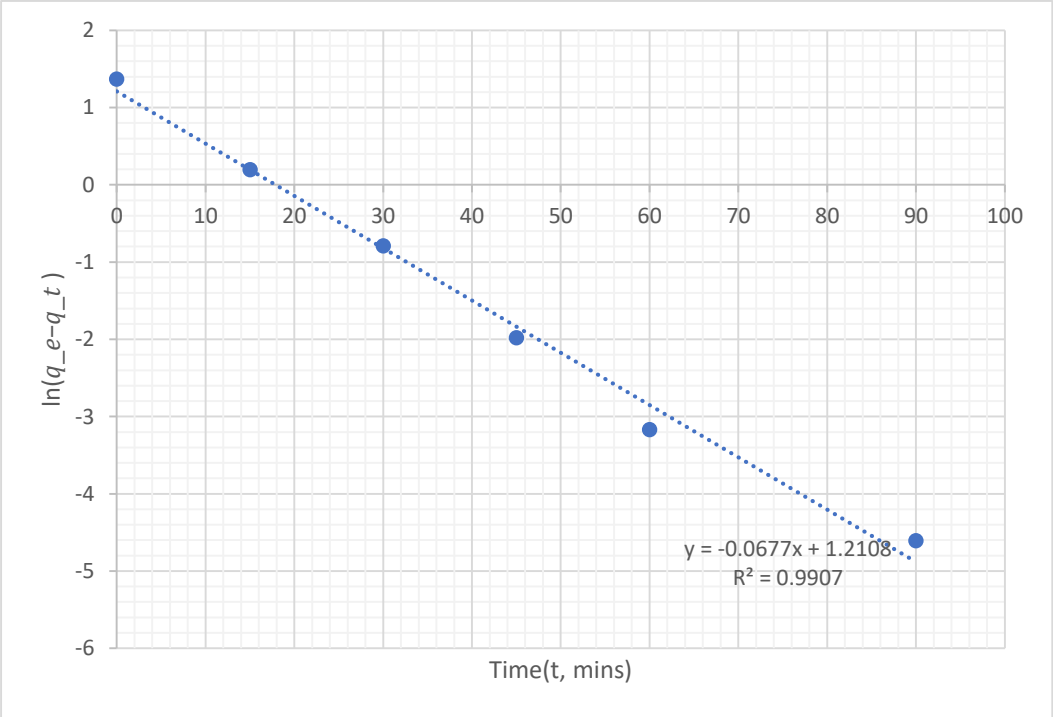

Figure 5: Pseudo-First-Order (PFO) kinetic plot displaying the regression line of $\ln(qe - qt)$ against contact time (t).

The mathematical modeling the linear PFO expression is governed by Equation (6):

$q_t = \ q_e(1 - e^{-k_1 t}) \leftrightarrow \ln(q_e - q_t) = \ln(q_e) - k_1 t$ …..(Eq.6)

Applying a linear regression to the coordinates in Table 4 (as mapped in Figure 4) yields a slope ($-k_1$) of -0.0677min^{-1} and a y-intercept $\ln(q_e)$. This provides a calculated theoretical equilibrium capacity:

Calculated equilibrium adsorption capacity,

$$q_e = e^{1.2108}$$

$$= 3.3562 \text{ mg/g.}$$

While the PFO regression coefficient appears high, the calculated theoretical loading value (3.3562 mg/g) deviates substantially from the actual experimental value of 3.934 mg/g recorded in Table 4. This clear mathematical mismatch demonstrates that the system does not follow pseudo-first-order boundaries, proving that the extraction process is not controlled by simple, physical mass-transfer diffusion

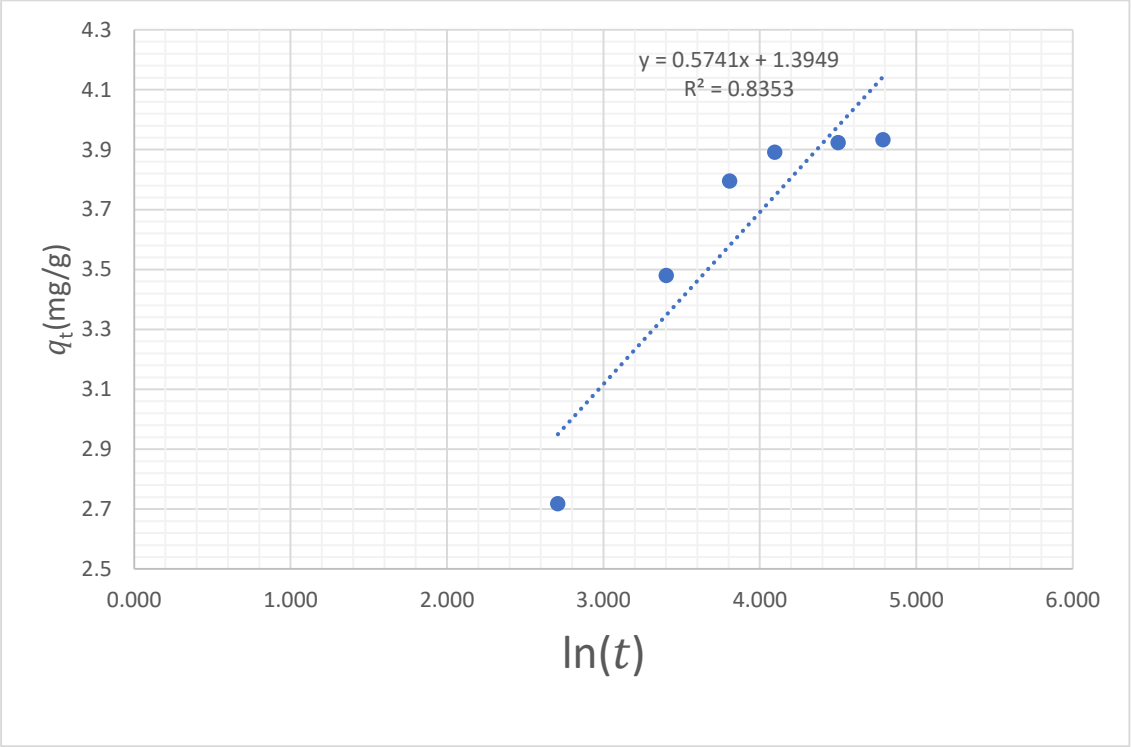

Figure 6: Elovich kinetic model evaluation curve plotting solid phase loading q_t against $\ln(t)$.

Similarly, the integrated Elovich model, which evaluates multi-mechanistic loading across heterogeneous surfaces via Equation (7), was fitted by plotting $q_t$against $\ln(t)$in Figure 5:

$$q_t = \frac{1}{\beta}\ln(\alpha\beta) + \frac{1}{\beta}\ln(t) \ldots\ldots \textbf{(Eq.7)}$$

The Elovich correlation coefficient yielded a poor linear fit (R^2 = 0.8353), as plotted in Figure 5. This low correlation confirms that the adsorption rate is not driven by an exponential decrease in variable active sites across an energetically heterogeneous matrix, eliminating the Elovich model from the primary rate-controlling description

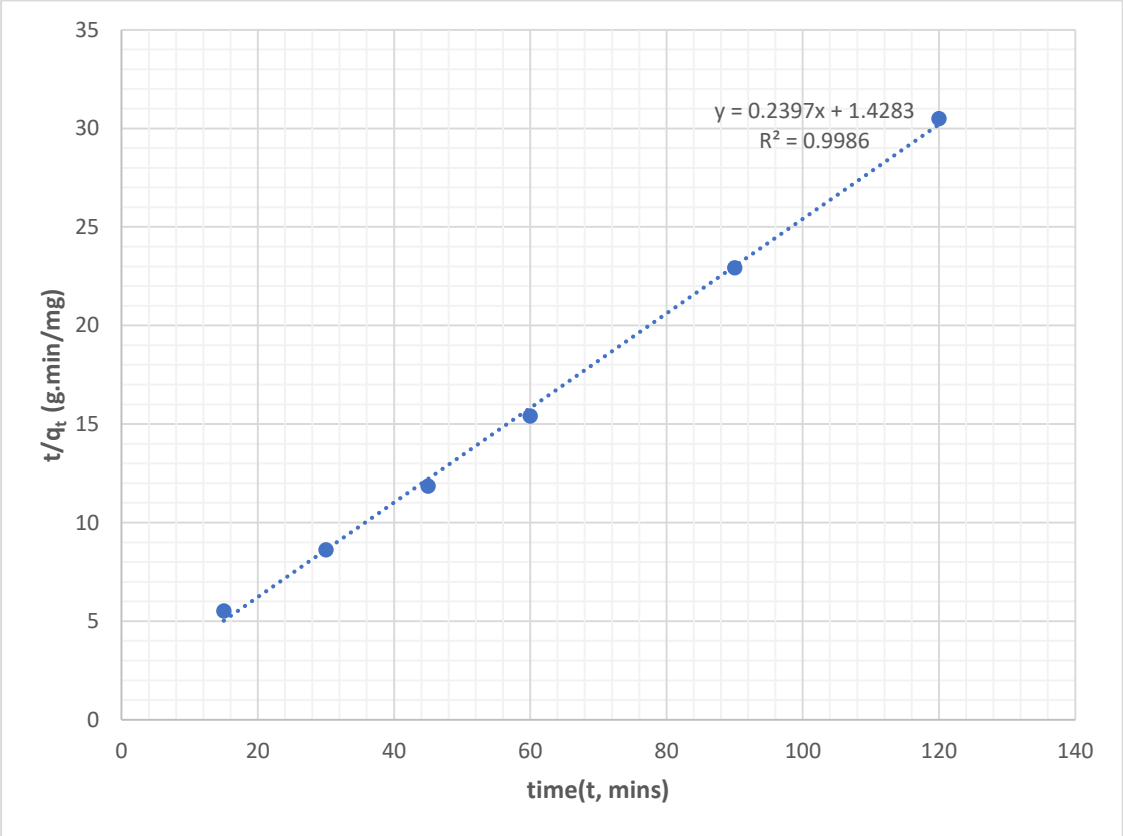

Figure 7: Pseudo-Second-Order (PSO) kinetic plot displaying the linear fit of (t/qt) against time (t).

In stark contrast, the experimental data shows an exceptional fit when modeled under Pseudo-Second-Order (PSO) parameters. The mathematical framework for the linearized PSO coordinate system is governed by Equation (8):

$$\frac{t}{q_t} = \frac{1}{K_{2q_e^2}} + \frac{1}{q_e}t \ldots. \textbf{(Eq.8)}$$

By plotting the final column coordinates ($\frac{t}{q_t}$) from Table 3 against contact time (t) in Figure 2, the system yields a near-perfect linear regression equation:

$$y = 0.2397 + 1.4283 \ \ (R^2 = 0.9986)$$

The slope of the line corresponds directly to$\frac{1}{q_e}$, while the y-intercept matches $\frac{1}{K_2 q_e{}^2}$. Solving for the theoretical equilibrium capacity (q_e) yields:

$\boldsymbol{q_e}$(Theoretical) = $\frac{1}{slope}$ = $\frac{1}{0.2397}$ = 4.17mg/g

This calculated capacity (4.17mg/g) matches your experimental maximum value of 3.934 mg/g with high precision. To evaluate the operational velocity, the pseudo-second-order rate constant (k_2) was derived from the intercept value (1.4283) using the formula:

$\boldsymbol{K_2} = \frac{\boldsymbol{Slope^2}}{\boldsymbol{intercept}} \boldsymbol{K_2} = \frac{(\mathbf{0.2397^2})}{\mathbf{1.4283}}$

= 0.0402g/mg.min

Using these parameters, the initial adsorption rate (h) as t →0 was calculated from the inverse of the intercept:

$$h = \boldsymbol{K_2} \times q_e{}^2$$

$= \frac{\mathbf{1}}{\boldsymbol{intercept}} = \frac{1}{1.4283}$= *0.7001mg/(g.min)*

The near-perfect correlation coefficient (R^2= 0.9986) and the close agreement between the theoretical and experimental capacities provide definitive mathematical proof that the system is governed by the pseudo-second-order model. This confirms that the rate-limiting step is a chemisorption pathway. The extraction of SLS from wastewater does not rely on weak physical accumulation; instead, it is driven by strong chemical interactions involving electron sharing or electrostatic valency pairing between the functional groups of the acid-activated carbon and the surfactant molecules.

4.5 Adsorption Isotherm Modeling

To map the equilibrium boundary layer and quantify the maximum surface loading characteristics, steady-state batch extractions were analyzed across varying initial SLS concentrations (10 to 40 mg/L). The empirical relationships combining residual concentration (c_e), removal efficiency ($R, \%$), and equilibrium solid-phase capacity (q_e) are compiled in **Table 5.**

Table 5: Equilibrium data for SLS adsorption capacity across varying initial concentration levels.

Initial concentration ($C_i, mg/l$)	Absorbance	Equilibrium concentration ($c_e, mg/l$)	Removal (%)	Adsorption capacity($q_e, mg/g$)
10	0.014	0.20	98.0	1.96
15	0.017	0.25	98.3	2.95
20	0.022	0.33	98.3	3.93
25	0.051	0.80	96.8	4.84
30	0.089	1.40	95.3	5.72
35	0.140	2.20	93.7	6.56
40	0.222	3.50	91.3	7.30

The data in Table 5 highlights a critical thermodynamic trend. As the initial concentration of SLS rises from 10mg/L to 40mg/L, the solid-phase equilibrium capacity scales upward from 1.96mg/g to 7.30mg/g. This increase is driven by a stronger concentration gradient, which increases the driving force to push surfactant molecules from the liquid phase onto the carbon surface. Concurrently, the overall removal efficiency drops from a peak of 98.3% down to 91.3%, indicating that the active surface sites are approaching complete saturation.

To understand the nature of this surface coverage, the data points were fitted to the Langmuir and Freundlich isotherm models (Figure 8 and 9). The Langmuir framework assumes uniform monolayer adsorption onto a completely homogeneous surface with no lateral interaction between adsorbed molecules. The linearized form of this model, using Hanes-Woolf coordinates

($\frac{C_e}{q_e}$vs.C_e) is calculated via Equation (9) and compiled in Table 6.

$$\frac{C_e}{q_e} = \frac{1}{Q_m} C_e + \frac{1}{Q_e k_L} \ldots\ldots \text{(Eq.9)}$$

Table 6: Linearized data coordinates compiled for the Hanes-Woolf Langmuir isotherm model expression.

Equilibrium concentration(C_e , mg/l)	$\frac{C_e}{q_e}$
0.2	0.10
0.25	0.08
0.33	0.08
0.8	0.17
1.4	0.24
2.2	0.34
3.5	0.48

Plotting these coordinates in Figure 6 generates a clear linear regression line with the equation $y = 0.121x + 0.0636$, yielding an exceptionally high correlation coefficient ($R^2 = 0.9932$). The absolute maximum monolayer capacity (Q_m)was derived from the reciprocal of the slope:

Maximum capacity $(Q_m) = \frac{1}{slope} = \frac{1}{0.121}$= 8.2645mg/g

The Langmuir affinity constant(K_L), which evaluates the balance between the adsorption and desorption rates, was computed using both the slope and the y-intercept (0.0636):

Langmuir constant (K_L) = $\frac{1}{Slope \times intercept} = \frac{1}{0.121 \times 0.0636}$ = 129.944 L/mg

This high $K_L$value (129.944L/mg) demonstrates a strong chemical affinity between the sawdust activated carbon matrix and the surfactant adsorbate. To verify the favorability of this process, the dimensionless separation factor (R_L) was evaluated across the entire concentration range via Equation (9.1):

$$R_L = \frac{1}{1 + K_L C_i} \ldots\ldots Eq(9.1)$$

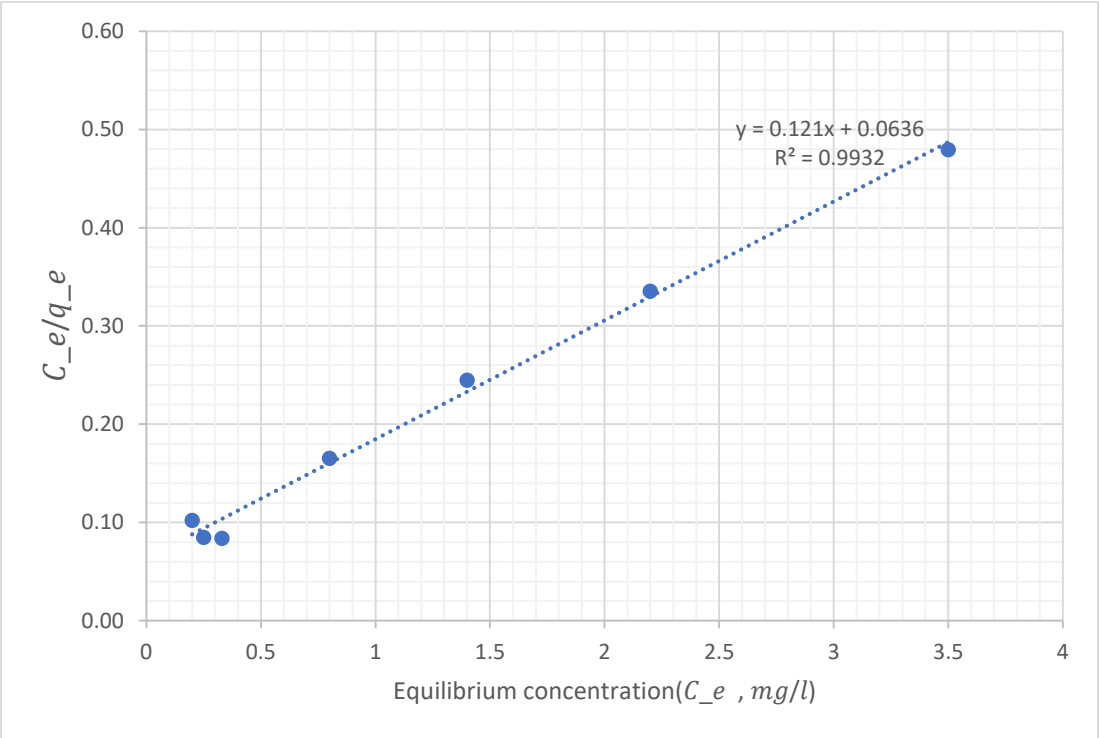

Figure 8: Langmuir isotherm linear regression plot mapping coordinates of $\left(C_e/q_e\right)$ ***versus equilibrium concentration*** (C_e)***.***

Substituting your lowest initial concentration ($C_i = 10mg/l$) into Equation (9.1) yields R_L of 0.00077, while a baseline reference loading ($C_i = 10mg/l$) gives R_L = 0.071. Because these calculated $R_L$values fall within the strict thermodynamic boundary of 0 <R_L< 1, the adsorption process is highly favorable, confirming a highly efficient chemisorption mechanism.

To verify this homogeneous surface theory, the datasets were also fitted to the logarithmic Freundlich model via Equation (10), which evaluates multilayer accumulation across heterogeneous energetic grids. The transformed logarithmic coordinates are compiled in Table 7 and plotted in Figure 7.

$$\log q_e = \log K_f + \frac{1}{n}\log C_e \ldots\ldots \textbf{(Eq.10)}$$

Table 7: Logarithmic parameter values compiled for verification of the Freundlich isotherm equation.

Equilibrium concentration($c_e, mg/l$)	Adsorption capacity($q_e, mg/g$)	$\log c_e$	$\log q_e$
0.2	1.96	-0.6990	0.2923
0.25	2.95	-0.6021	0.4698
0.33	3.93	-0.4815	0.5944
0.8	4.84	-0.0969	0.6848
1.4	5.72	0.1461	0.7574
2.2	6.56	0.3424	0.8169
3.5	7.30	0.5441	0.8633

The resulting linear equation from Figure 7 (y = 0.3947x + 0.6876) yields a correlation coefficient ($R^2 = 0.8915$). The relative adsorption intensity (n) was solved from the inverse of the slope:

Adsorption intensity $(n) = \frac{1}{0.3947}$ = 2.534

While the value of n falls between 1 and 10 (confirming an operationally favorable configuration), the Freundlich capacity constant (K_f) was derived from the intercept value (0.6876):

$\log K_f$ = 0.6876, $K_f = 10^{0.6876}$ = 4.871 $(mg/g)(L/mg)^{1/n}$

Comparing the two models, the Langmuir correlation parameter ($R^2 = 0.9932$) is significantly higher than the Freundlich coefficient (R^2 = 0.8915). This definitive mathematical comparison proves that the system follows the Langmuir monolayer theory. Adsorption takes place on a highly uniform, homogeneous surface where all active binding sites are energetically identical, and coverage is strictly limited to a single layer of molecules.

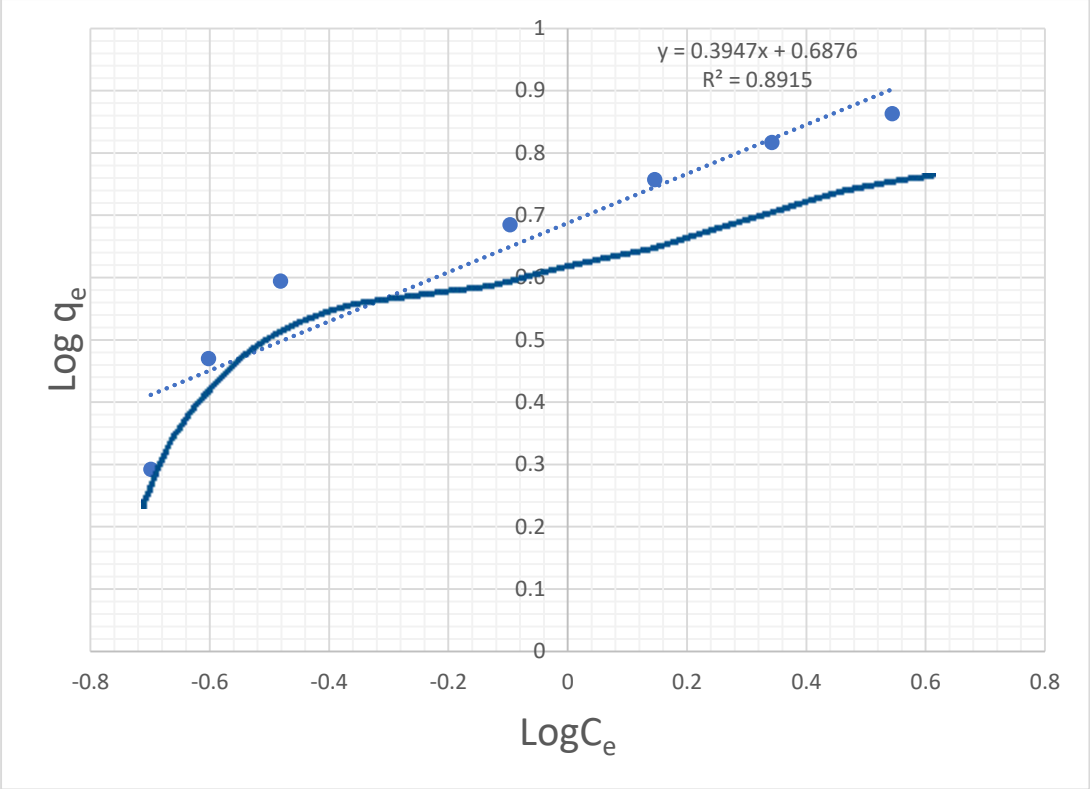

Figure 9: Freundlich isotherm linear plot tracking $log(q_e)$ versus $log(C_e)$ illustrating surface deviations...

4.6 Influence of Operational Parameters.

4.6.1 Effect of solution pH and structural FTIR coupling

The impact of initial pH (pH_i) on the extraction efficiency was evaluated between pH 2.0 and 12.0 using a constant SLS loading of 20mg/L and an adsorbent dose of 0.5g/L over a 120-minute contact period. The operational metrics are compiled in Table 8 and visually mapped in Figure 8.

***Table 8: Influence of solution initial pH** variations **on equilibrium SLS concentration, removal efficiency, and final pH**.*

Initial (PH_i)	Absorbance	Equilibrium concentration$(c_e, mg/l)$	Removal, (R, %)	Adsorption capacity$(q_e, mg/g)$	Final (PH_f)
2.0	0.007	0.10	99.5	3.98	2.8
4.0	0.011	0.16	99.2	3.97	5.2
6.0	0.022	0.33	98.3	3.93	6.4
8.0	0.102	1.60	92.0	3.68	7.2
10.0	0.222	3.50	82.5	3.30	8.5
12.0	0.379	6.00	70.0	2.80	10.6

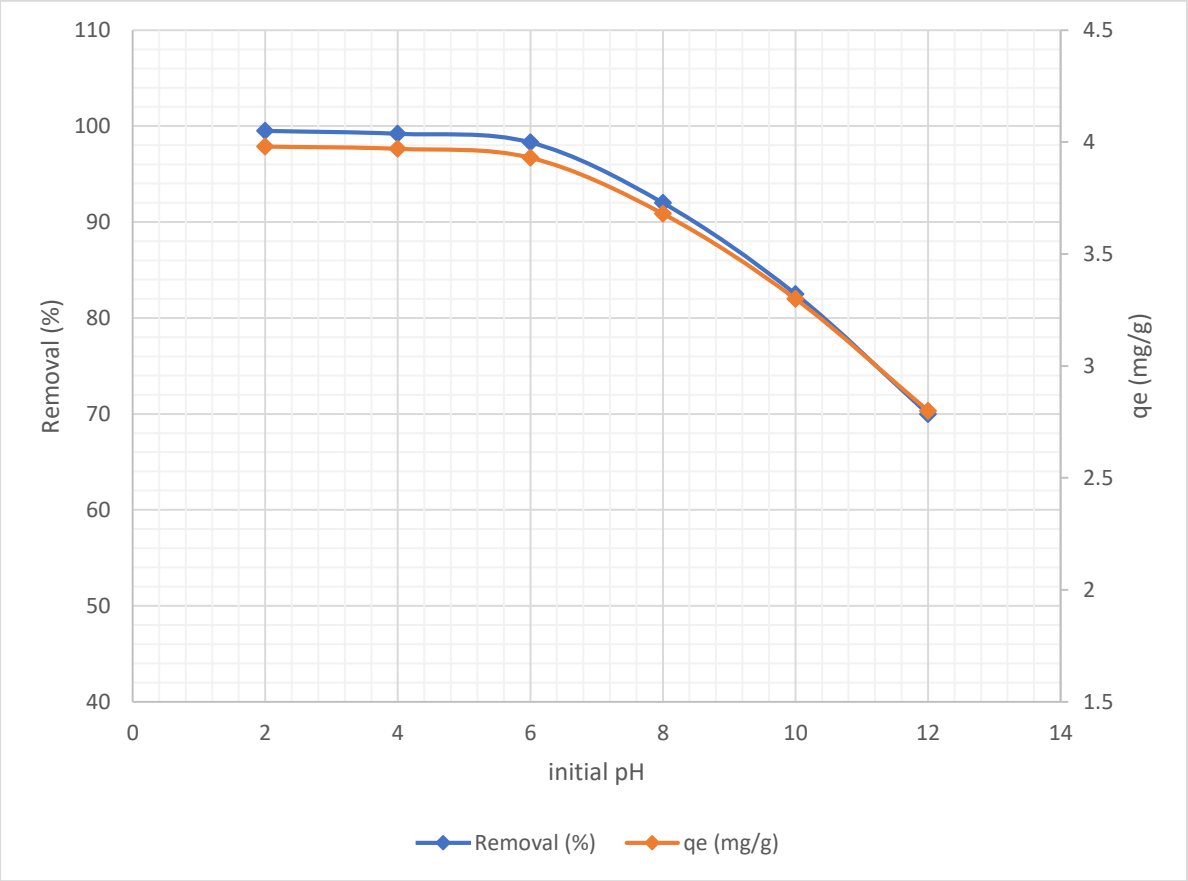

***Figure 10: Performance profiles highlighting the influence of initial solution pH on SLS removal efficiency (%) and adsorption capacity** (q_e).*

The data in Table 8 reveals exceptionally strong pH dependence. The maximum removal efficiency occurs at an acidic value of pH 2.0, reaching 99.5 % (q_e= 3.98mg/g), maintaining an elite extraction plateau above 98% across the entire acidic range (pH 2.0 to 6.0). However, a significant drop occurs once the solution passes pH 6.0. Between pH 6.0 and 12.0, the overall removal efficiency drops sharply by nearly 30%, falling to 70.0 %(q_e= 2.80mg/g),

To explain this performance shift, FTIR spectroscopic features provide the necessary chemical context. The prominent FTIR bands recorded by the JASCO instrument confirm that the phosphoric acid activation successfully introduced key oxygen/phosphorus functional groups onto the graphitic surface:

3280cm^{-1}: Confirms abundant surface hydroxyl (-OH) stretching nodes.

1600cm^{-1}: Represents aromatic C=C backbones mixed with conjugated carbonyl (C=O) receptors.

1060cm^{-1}: Validates the incorporation of phosphorus-containing bands (P=O, P-O linkages, and P-O-H stretching vectors).

These functional groups undergo protonation or deprotonation depending on the solution pH, which is directly controlled by the adsorbent's Point of Zero Charge (pH_{pzc}).Plotting PH_fagainst PH_iin Figure 9 identifies the exact pH_{pzc} where the overall net electrical charge of the carbon surface equals zero:

$$pH_{pzc} = 6.2 \ldots [Fromfig.9\ Axiscross]$$

This pH_{pzc}value of 6.2 mathematically explains the multi-mechanistic behavior summarized in Table 9:

Table 9: Mechanistic matrix summarizing primary interactions and surface alignment across acidic, neutral, and basic pH domains.

pH range	Primary interaction	Surface state	SLS Alignment
Acidic (2-6)	Electrostatic + hydrophobic	Positive (+)	Head – down(strong)
Neutral (6.0)	Hydrogen bonding + hydrophobic	Neural (0)	Mixed
Basic (8-12)	Hydrophobic	Negative (-)	Tail –down (weaker)

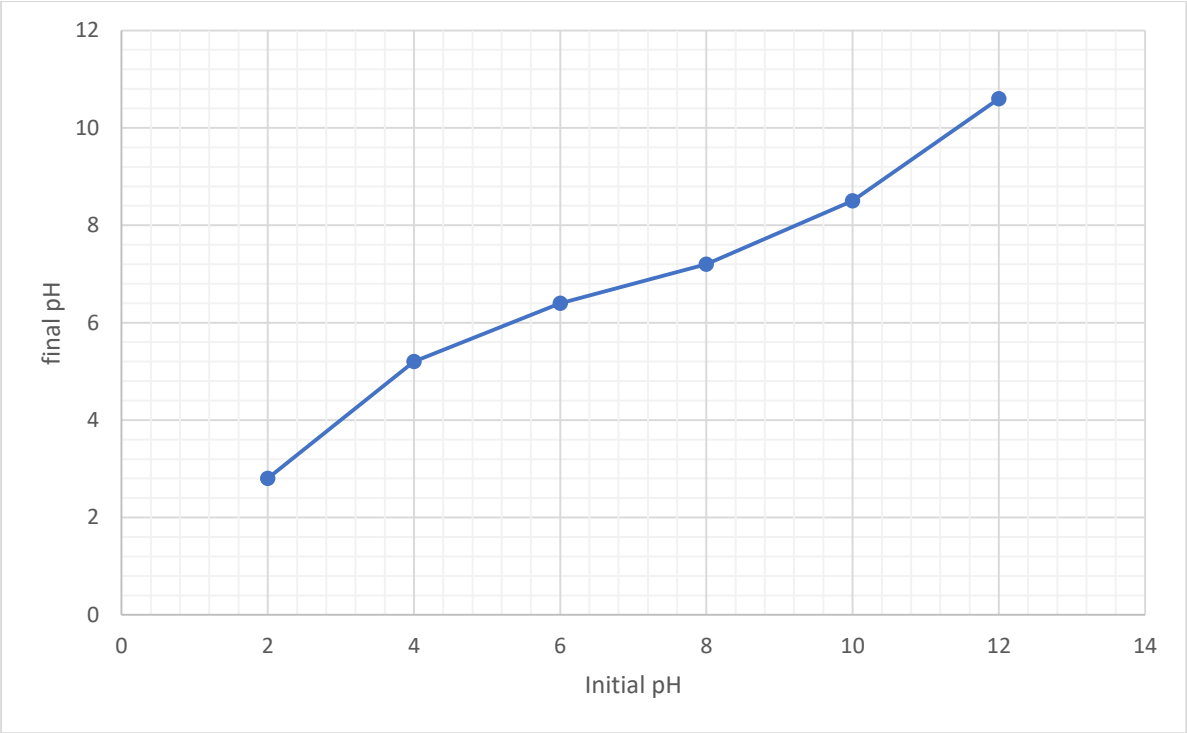

Figure 11: Potentiometric cross-plot for estimating the point of zero charge (pH_{pzc}) of the acid-activated sawdust carbon.

Electrostatic Attraction (Dominant at Low pH): When solution pH is below pH_{pzc} (pH 2.0 - 6.0 < 6.2), an abundance of hydronium ions (H^+) protonates the active functional nodes (-OH at 3280$cm^{-1}$and P-O-H configurations at 1060cm^{-1}), rendering the carbon surface highly positive. This generates a powerful electrostatic draw with the negative sulfate heads (OSO_3) of the SLS molecules, driving the peak 99.5% extraction efficiency.

Hydrophobic Association (Dominant at High pH): When solution pH sits above pH_{pzc} (pH 8.0 - 12.0 > 6.2), hydroxide ions (OH^-) deprotonate these functional clusters, creating a net negative surface charge. This induces electrostatic repulsion with the anionic surfactant heads. However, the system still achieves a notable 70% removal at pH 12.0. This sustained performance is driven by hydrophobic interactions, where the non-polar 12-carbon alkyl tail of the SLS molecule aggregates onto the hydrophobic graphitic planes (confirmed by the aromatic C=C peak at $1600 cm^{-1}$) via London dispersion forces to escape the water phase.

Hydrogen Bonding: Additionally, the oxygen atoms in the SLS sulfate heads form stable hydrogen bonds with any remaining un-ionized hydroxyl or carboxylic groups on the carbon surface, providing secondary anchor points that stabilize the uniform monolayer coverage.

4.6.2 Effect of Adsorbent Dosage Optimization

To determine the most cost-effective mass ratio, the adsorbent dosage was varied from 0.5 g/L to 5.0g/L at a constant initial SLS concentration of 20mg/L and an optimal operational pH of 4.0. The resulting extraction metrics are compiled in Table 10 and mapped visually in Figure 10

Table 10: Operational metrics documenting the effect of increasing absorbent dosage metrics on SLS extraction performance.

Adsorbent dosage(□/□)	Adsorbent mass(□)	□□(□□/□)	Removal(%)	□□(□□/□)
0.5	0.05	11.20	44	17.60
1.0	0.10	4.80	76.0	15.20
2.0	0.20	0.55	97.2	9.72
3.0	0.30	0.12	99.4	6.63
4.0	0.40	0.05	99.7	4.98
5.0	0.50	0.02	99.9	3.99

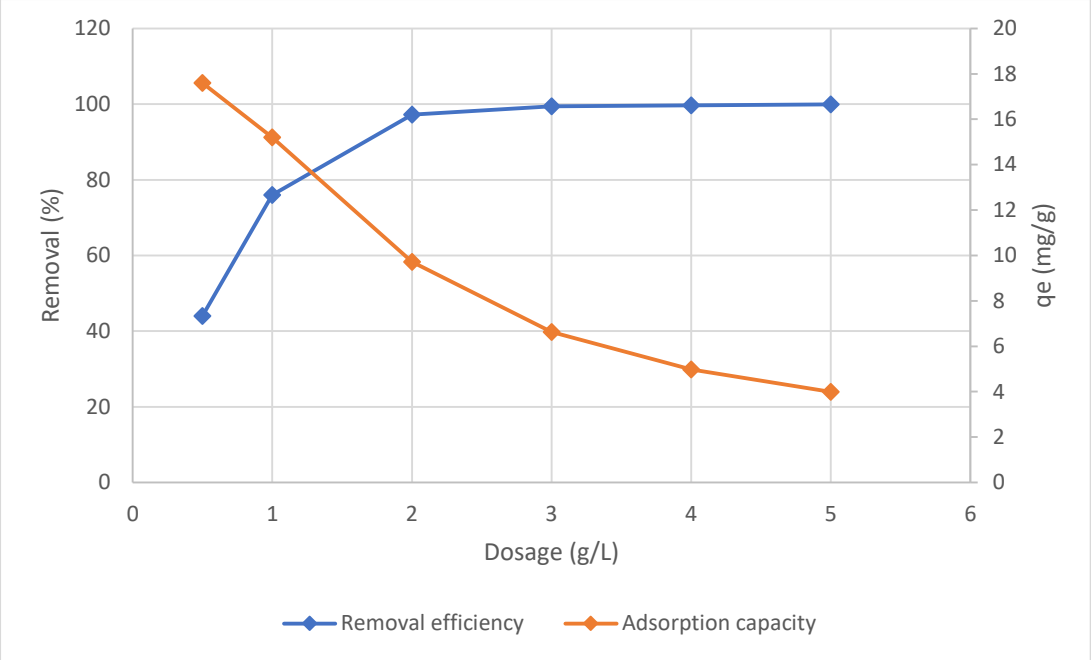

Figure 12: Optimization profile showing the impact of adsorbent dosage on total removal percentage and individual equilibrium loading (□□).

The optimization metrics in Table 10 outline two opposing trends. As the dosage increases from 0.5 g/L to 5.0 g/L, the total removal efficiency rises sharply from 44% to 99.9%, driven by the larger total surface area and the greater number of available active binding sites. Conversely, the individual solid-phase capacity (□□) drops from a maximum of 17.60 mg/g down to 3.99 mg/g. At the lowest dosage (0.5 g/L), the high loading value (17.60 mg/g) significantly exceeds the calculated Langmuir monolayer limit (□□ = 8.264 mg/g), which confirms that at very low adsorbent-to-solute ratios, the surfactant molecules form aggregate clusters or "hemi-micelles" on the crowded carbon surface.

As illustrated in Figure 10, the mathematical intersection where the removal efficiency and individual capacity curves balance out occurs at approximately 1.3 g/L. However, the true Practical Optimum Dosage is 2.0 g/L, where near-complete extraction (97.2%) is achieved without unnecessary material waste or site underutilization observed at higher dosages. The final consolidated performance limits are summarized in Table 11.

Table 11: Consolidated optimization summary report highlighting critical thresholds, operational limits, and peak observed parameters.

Property	Value/Observation
Balance Point Dosage	~1.3 g/L
Optimum Practical Dosage	2.0 g/L
Max Removal Observed	~99.5% (at 5.0 g/L)
Max Capacity Observed	~17.5 mg/g (at 0.5 g/L)

To validate the operational performance of the synthesized sawdust bio-adsorbent, its peak parameters were compared with alternative biomass-derived activated carbons evaluated in recent literature. The maximum monolayer adsorption capacity (Q_{max} = 8.26mg/g) matches performance baselines recorded for non-modified agricultural waste remnants. The extreme sensitivity to acidic conditions, where removal peaks at 99.5% at pH 2.0, aligns with traditional surfactant extraction matrices. At low pH domains below the point of zero charge (pH_{pzc} = 6.2), the highly protonated carbon matrix undergoes strong electrostatic attraction with the negative hydrophilic head group (OSO_3^-) of the incoming SLS molecules. While commercial chemical adsorbents display higher absolute capacity metrics due to expensive synthetic chemical doping treatments, this locally derived sawdust framework delivers cost-effective extraction performance. This makes it an ideal engineering choice for resource-limited industrial wastewater treatment frameworks.

CHAPTER FIVE: CONCLUSION AND RECOMMENDATIONS

5.1 Conclusion

Based on the comprehensive experimental findings and mathematical modeling generated in this research project, the following core conclusions are established:

Successful Structural Synthesis: Locally sourced sawdust biomass from the Tororo region was successfully transformed into highly active microporous activated carbon via phosphoric acid chemical activation at *800℃*. This was proven by an exceptional standardized iodine number of approximately 940mg/g.

Functional Backbone Verification: FTIR spectroscopy verified successful surface functionalization, showing prominent hydroxyl stretches (3280$\square\square^{-1}$), aromatic backbones (1600$\square\square^{-1}$), and a rich acid-phosphate ester network (1200$\square\square^{-1}$ - 900$\square\square^{-1}$), which set up an optimal surface point of zero charge ($\square\square_{\square\square\square} = 6.2$).

Chemisorption Rate Mechanics: The dynamic phase extraction follows the Pseudo-Second-Order kinetic model ($\square^2$ = 0.9986), proving that strong chemisorption chemical valency sharing acts as the primary rate-controlling mechanism.

Homogeneous Monolayer Boundaries: Steady-state equilibrium boundaries strictly fit the Langmuir isotherm model ($\square^2$ = 0.9932), showing completely uniform monolayer binding with a maximum absolute loading capacity ($\square_\square$) of 8.2645 mg/g and high binding favorability ($0 < \square_\square < 1$).

Multi-Mechanistic pH and Mass Optimization: Batch treatment processes are highly sensitive to solution parameters. Peak removal (99.5%) occurs under acidic boundaries (pH 2.0) via powerful electrostatic attraction, while a practical optimum dosage of 2.0g/L ensures excellent removal 97.2% without material waste.

5.2 Recommendations

To build upon the insights gained from this study and advance the engineering application of this biomass-derived adsorbent, the following steps are recommended:

Continuous-Flow Column Scaling: Transition from static batch-scale extractions into continuous fixed-bed flow column configurations to calculate critical industrial parameters, including break-through times; mass transfer zones, and exhaustion limits.

Real Industrial Wastewater Evaluation: Test the manufactured sawdust carbon using genuine industrial or textile wastewater effluents from Ugandan factories to evaluate how co-existing competitive ions, organic materials, and true chemical matrix variations affect actual SLS removal yields.

Desorption and Regeneration Characterization: Conduct elution assays using varied solvent matrices (such as dilute ethanol or alkaline solutions) to evaluate the structural recyclability, chemical reusability, and long-term economic lifecycle of the carbon adsorbent.

Surface Modification Expansions: Investigate secondary chemical modifications, including surface doping or surfactant-tailoring, to further enhance the maximum monolayer adsorption capacity (□□) under alkaline and neutral pH conditions.

5.3 Areas for Further Research

To build on this study, future research should focus on the following areas. Surface Morphology and Pore Structure (SEM): Since this study did not include Scanning Electron Microscopy (SEM), future work should use SEM to visually assess the surface morphology, roughness, and pore structure of the sawdust carbon before and after surfactant trapping.

Testing with Mixed Pollutants: Future projects should examine how this carbon behaves when multiple pollutants are present in the water simultaneously, as other chemicals and minerals might compete for the same binding sites.

Continuous Flow Column Testing: Instead of testing small batches in beakers, future work should test the carbon in a continuous-flow column to assess its performance in treating large volumes of flowing wastewater.

Temperature and Energy Tests: Future experiments should test the process at different temperatures to quantify the exact thermodynamic energy changes and determine whether the process performs better under hot or cold conditions.

Cost and Environmental Analysis: A comprehensive study should be conducted to calculate the exact financial cost and environmental impact of producing this carbon using phosphoric acid at high temperatures on a factory scale.

Cleaning and Reusing the Carbon: More research is needed to find the best way to wash and reuse the dirty carbon multiple times without destroying its internal.

REFERENCES

1. Arnelli, Aditama, W. P., Fikriani, Z., & Astuti, Y. (2018). Adsorption kinetics of surfactants on activated carbon. *IOP Conference Series: Materials Science and Engineering*, *349*(1). https://doi.org/10.1088/1757-899X/349/1/012001
2. Baari, M. J., Rudi, L., & Harimu, L. (2025). Adsorption isotherms, thermodynamics, and kinetics of activated carbon as adsorbent to water pollutants: a review. *Chimica Techno Acta*, *12*(12214), 1–25. https://doi.org/10.15826/chimtech.2025.12.2.14
3. Cataldo, S., Muratore, N., Giannici, F., Bongiorno, D., Chiodo, V., Maisano, S., & Pettignano, A. (2022). Hydrocarbons removal from synthetic bilge water by adsorption onto biochars of dead Posidonia oceanica. *Environmental Science and Pollution Research*, *29*(60), 90231–90247. https://doi.org/10.1007/s11356-022-21998-x
4. Elboughdiri, N., Iqbal, S., Abdullaev, S., & Aljohani, D. M. (2025). RSC Advances Correction and removal of expression of concern : Enhanced electrical and magnetic properties of (Co , Yb) co-doped ZnO memristor for. *RSC Advances*, *15*, 8876–8877. https://doi.org/10.1039/D5RA90029H
5. Hartal, O., Haddaji, C., & Anouzla, A. (2023). *Recent Advances in Physicochemical and Biological Techniques for the Management of Discharges Loaded with Surfactants*. *37*(1), 1–16.
6. Hokkanen, S., Bhatnagar, A., Koistinen, A., Kangas, T., Lassi, U., & Sillanpää, M. (2018). Comparison of adsorption equilibrium models and error functions for the study of sulfate removal by calcium hydroxyapatite microfibrillated cellulose composite. *Environmental Technology (United Kingdom)*, *39*(8), 952–966. https://doi.org/10.1080/09593330.2017.1317839
7. Khalid, M. W., & Salman, S. D. (2019). *Adsorption of Chromium Ions on Activated Carbon Produced from Cow Bones*. *20*(2), 23–32.
8. Lechuga, M., Fernández, M., Francisco, S., Alejandro, R., & Arteaga, F. (2022). Environmental impact assessment of nanofluids containing mixtures of surfactants and silica nanoparticles. *Environmental Science and Pollution Research*, 84125–84136. https://doi.org/10.1007/s11356-022-21598-9
9. Malik, 2004. (2009). *LOW-COST MUNICIPAL WASTEWATER TREATMENT OPTIONS FOR USE IN PAKISTAN – A REVIEW*. *15*(1), 71–78.

10. Maria, A. S., & Florence, N. (2020). *Purification of Zinc Contaminated Water Using Activated Carbon , Banana and Orange Peels from Katalina Spring Banda- Nakawa Division Kampala District*. *15*(5), 1–5. https://doi.org/10.9790/3008-1505060105
11. Oladimeji, T. E., Odunoye, B. O., Elehinafe, F. B., Obanla, O. R., & Odunlami, O. A. (2021). Production of activated carbon from sawdust and its efficiency in the treatment of sewage water. *Heliyon*, *7*(1), e05960. https://doi.org/10.1016/j.heliyon.2021.e05960
12. Pimentel, C. H., Freire, M. S., Gómez-Díaz, D., & González-Álvarez, J. (2024). Continuous Adsorption of Acid Wood Dyes onto an Activated Carbon Prepared from Pine Sawdust. *Applied Sciences (Switzerland)*, *14*(2). https://doi.org/10.3390/app14020841
13. Quispe, J. I. B., Campos, L. C., Mašek, O., & Bogush, A. (2024). *Removal of anionic surfactant from aqueous solutions by adsorption onto biochars : characterisation , kinetics , and mechanism*. *3330*. https://doi.org/10.1080/09593330.2024.2304677
14. Shaker, A. M., Khedawy, M., Moneer, A. A., El-Mallah, N. M., & Ramadan, M. S. (2025). Loading of anionic surfactant on eco-friendly biochar and its applications in Cr(VI) removal: adsorption, kinetics, and reusability studies. *BMC Chemistry*, *19*(1). https://doi.org/10.1186/s13065-024-01363-4
15. Torres-Castañón, L. A., Robledo-Peralta, A., Antileo, C., Silerio-Vázquez, F. de J., & Proal-Nájera, J. B. (2025). Sawdust-based adsorbents for water treatment: An assessment of their potential and challenges in heavy metal adsorption. *Journal of Hazardous Materials Advances*, *18*(March). https://doi.org/10.1016/j.hazadv.2025.100758
16. Wiśniewska, M., Tokarska, K., Urban, T., & Nowicki, P. (2025). Production of activated biocarbons by microwave - assisted chemical activation of hardwood sawdust and their application in the simultaneous removal of polymers of different origins from aqueous systems. *Wood Science and Technology*, *59*(1), 1–28. https://doi.org/10.1007/s00226-024-01623-5
17. Zachariou, V., Klatzky, R., & Behrmann, M. (2003). *nc or re ct Pr oo f nc or re ct ed Pr oo f. 17*, 1–21. https://doi.org/10.5812/ajehe.61902.Research

APPENDICES

APPENDIX A: Raw Analytical Calibration and Calibration Standards

A stock solution of Sodium Lauryl Sulfate (SLS) with a concentration of 1000 mg/L was prepared by dissolving exactly 1.000 g of high-purity SLS powder in 1000mL of deionized water inside a volumetric flask. Working calibration standards of 2.0, 4.0, 6.0, 8.0, and 10.0 mg/L were prepared through sequential serial dilutions of the stock solution. Each standard was mixed with Methylene Blue reagent and extracted using chloroform before measuring its light absorbance at 652 nm using the UV-Vis spectrophotometer.

APPENDIX B: Laboratory Apparatus and Experimental Setup

The experimental operations were performed using the following laboratory instrumentation:

JASCO FT/IR-6600 Spectrometer: Equipped with an ATR PRO ONE diamond crystal accessory for surface functional group analysis.

UV-Vis Spectrophotometer: Operated at a fixed wavelength of 652 nm using matching 10 mm quartz cuvettes.

Thermostatic Water Bath Shaker: Maintained at a constant agitation speed of 175 rpm for all kinetic and equilibrium batch runs.

Digital pH Meter: Calibrated daily using standard buffer solutions at pH 4.01, 7.00, and 10.01.

Real-time solid capacity values, and Equation (6) to set up the linear coordinates for the pseudo-second-order kinetic regression modeling.